

## Resonant Second-Order Nonlinear Optical Processes in Quantum Cascade Lasers

Nina Owschimikow,<sup>1</sup> Claire Gmachl,<sup>1</sup> Alexey Belyanin,<sup>2</sup> Vitaly Kocharovskiy,<sup>2</sup> Deborah L. Sivco,<sup>1</sup>  
Raffaele Colombelli,<sup>1</sup> Federico Capasso,<sup>1</sup> and Alfred Y. Cho<sup>1</sup>

<sup>1</sup>*Bell Laboratories, Lucent Technologies, 600 Mountain Avenue, Murray Hill, New Jersey 07974*

<sup>2</sup>*Department of Physics, Texas A&M University, College Station, Texas 77843*

(Received 13 August 2002; published 31 January 2003)

We demonstrate an efficient intracavity nonlinear interaction of laser modes in a specially adapted quantum cascade laser. A two-wavelength quantum cascade laser structure emitting at wavelengths of 7.1 and 9.5  $\mu\text{m}$  included cascaded resonant optical intersubband transitions in an intracavity configuration leading to resonantly enhanced sum-frequency and second-harmonic generation at wavelengths of 4.1, 3.6, and 4.7  $\mu\text{m}$ , respectively. Laser peak optical powers of 60 and 80 mW resulted in 30 nW of sum-frequency signal and 10–15 nW of second-harmonic signal, both in good agreement with theoretical calculations.

DOI: 10.1103/PhysRevLett.90.043902

PACS numbers: 42.65.Wi, 42.55.Px, 78.67.De, 85.35.Be

Advances in nonlinear optics continue to have a profound impact in new fields of physics as varied as the ultrashort pulse domain [1], slow light [2], microcavities [3], or quantum cryptography [4]. While nonlinear optical effects have been argued to be present even in few photon systems [5], most studies employ high power lasers as an external pump source and a nonlinear material for efficient generation of nonlinear optical radiation. Yet, even higher power conversion efficiency from the fundamental to the mixed light modes can be expected for a material that simultaneously acts as the pumping source and mixing nonlinearity. In addition, in this case all fields participating in the nonlinear interaction can be kept at an exact resonance with the corresponding transitions in a medium. This fact may lead to a peculiar interplay between effects of quantum coherence and nonlinear optical interactions, giving rise to exciting new physics at the intersection of nonlinear optics, quantum mechanics and optics, and laser dynamics.

In this Letter, we employ a quantum cascade (QC) laser [6] to demonstrate that intersubband (IS) optical transitions in stacked semiconductor quantum wells (QWs) can function as a simultaneous source of fundamental pump and nonlinearly generated light.

It was known from several pioneering works since the late 1980s that IS transitions in asymmetric single or coupled QWs can display giant nonlinear optical susceptibilities [7–13]. Recently, intracavity wave mixing has been proposed for interband semiconductor lasers [14] as an efficient mechanism to combine pump and mixing nonlinearity. Here, we show simultaneous intracavity sum-frequency and second-harmonic generation in two-wavelength QC lasers. First, the QWs of the QC-laser structures themselves can be designed to simultaneously support the required optical nonlinearities. This collocates the optically nonlinear region with the active laser waveguide core, allowing for a large overlap of the guided modes with the nonlinear region. Nevertheless,

the requirement of an equally optimized performance of the pump lasers may not always allow this approach. Therefore, a separate multiple QW section can be designed, which provides the necessary optical nonlinearity. This section is then inserted into the waveguide core between two stacks of QC lasers, again maximizing its overlap with the high optical power of the pump lasers. In both cases, the simultaneous IS nature of QC lasers and resonant optical nonlinearities automatically ensures optimized coupling of the fundamental pump radiation to the nonlinear medium.

We use a two-stack, two-wavelength ( $\lambda \sim 7.1$  and 9.5  $\mu\text{m}$ ) QC laser [15] and, sandwiched between the two laser stacks, a superlattice (SL) section. The  $\text{In}_{0.53}\text{Ga}_{0.47}\text{As}/\text{Al}_{0.48}\text{In}_{0.52}\text{As}$  heterostructure samples are grown by molecular beam epitaxy. A schematic of the layer sequence is shown in Table I. This structure provides two distinct sources of resonant second-order IS nonlinearities, one in the SL and one in the layer structure of the 7.1  $\mu\text{m}$  wavelength laser. Both means are schematically shown by the arrows in Figs. 1(a) and 1(b), respectively. In the SL [Fig. 1(a)], the first transition from the energy levels of the lowest miniband [“1” in Fig. 1(a)] to the localized states of the inserted QWs (“2”) is in near resonance with the radiation of the 9.5  $\mu\text{m}$  laser. The second transition, from these localized states (“2”) to the bottom of the second miniband (“3”), is near-resonant with the 7.1  $\mu\text{m}$  radiation.

In Fig. 1(b), the second set of resonant IS transitions is shown. While QC-laser action is taking place between energy levels “3” and “2” [6], near-resonant optical transitions of 9.5 and 7.1  $\mu\text{m}$  can be found from level “3” into level “4” and from the latter on to level “5,” respectively. We calculate the transition energies as  $\hbar\omega_{43} = 143$  meV,  $\hbar\omega_{54} = 164$  meV, and  $\hbar\omega_{53} = 307$  meV (where  $\hbar$  is the reduced Planck constant), and the corresponding optical dipole moments  $z_{43} = 0.7$  nm,  $z_{54} = 1.8$  nm, and  $z_{53} = 0.4$  nm. The line broadening at

TABLE I. Schematic stack sequence of a monolithic, two-wavelength QC laser with integrated resonant optical nonlinearities. Under operation electrons are traversing the stack from top to bottom. Thin (typically  $\sim 25$  nm) transition regions were inserted between individual building blocks to smooth out band discontinuities.

Layer type, doping level, and function	Thickness ( $\mu\text{m}$ )
InGaAs, $6 \times 10^{18} \text{ cm}^{-3}$ , outermost top waveguide cladding layer	0.5
AlInAs, $2 \times 10^{17} \text{ cm}^{-3}$ , top waveguide cladding layer	0.8
AlInAs, $1 \times 10^{17} \text{ cm}^{-3}$ , inner top waveguide cladding layer	2.8
InGaAs, $3 \times 10^{16} \text{ cm}^{-3}$ , top waveguide core layer	0.2
19 QC-laser active regions and injectors for emission at $9.5 \mu\text{m}$ wavelength [16], $1.9 \times 10^{11} \text{ cm}^{-2}$ per period	0.95
27-period modulated SL, $3 \times 10^{16} \text{ cm}^{-3}$ , includes resonant IS	0.22
16 QC-laser active regions and injectors for emission at $7.1 \mu\text{m}$ wavelength [16], $2.0 \times 10^{11} \text{ cm}^{-2}$ per period, includes resonant IS nonlinearity for SFG and SHG	0.75
InGaAs, $5 \times 10^{16} \text{ cm}^{-3}$ , buffer and bottom waveguide core layer	0.5
InP substrate, $\leq 4 \times 10^{17} \text{ cm}^{-3}$ , bottom waveguide cladding	$\sim 200$

the pump frequencies is about 10 meV, and at a mixing frequency it is 20–30 meV.

We can now estimate the second-order nonlinear susceptibility using the density-matrix approach, i.e., solving six equations for the density-matrix elements coupled with three wave equations for the fundamental pump fields of amplitude  $E_1$ ,  $E_2$ , and the mixing field  $E_3$ . We will give here the result only for the  $7.1 \mu\text{m}$  QC-laser region of Fig. 1(b), which provides a larger optical nonlinearity than the SL. The amplitude of the nonlinear polarization at a mixing wavelength of  $4.1 \mu\text{m}$  (the sum-frequency signal) is expressed via the amplitude of a corresponding off-diagonal element  $\sigma_{53}$  of a density matrix as  $P_{NL} = eN_e z_{53} \sigma_{53}$ , where  $e$  is the electron charge,  $N_e$  is electron density,

$$\sigma_{53} \cong e_1 e_2 \left( \frac{n_4 - n_5}{\Gamma_{54}} - \frac{n_3 - n_4}{\Gamma_{43}} \right) \left( \Gamma_{53} + \frac{|e_1|^2}{\Gamma_{54}} + \frac{|e_2|^2}{\Gamma_{43}} \right)^{-1}. \quad (1)$$

$\Gamma_{43} = \gamma_{43} + i(\omega_{43} - \omega_1)$ ,  $\Gamma_{54} = \gamma_{54} + i(\omega_{54} - \omega_2)$ , and  $\Gamma_{53} = \gamma_{53} + i(\omega_{53} - \omega_1 - \omega_2)$  are the complex line broadenings of the corresponding transitions,  $\omega_{1,2}$  the frequencies of the pump laser fields, and  $e_1 = ez_{43}E_1/\hbar$  and  $e_2 = ez_{54}E_2/\hbar$  the Rabi frequencies of the pump fields. The normalized electron densities  $n_{3,4,5}$  in states 3, 4, and 5 are not free parameters and must be found from the same set of equations, as it is done in [14] for intracavity mixing in interband lasers. We furthermore use the common approximation in QC lasers [6] that only the upper laser level “3” and the ground state of the injector [“g” in Fig. 1(b)] are significantly populated during laser operation.

Using the calculated parameters of all IS transitions, the resulting second-order optical susceptibility can be estimated as  $|\chi^{(2)}| \approx 8 \times 10^{-7} (N_3/10^{16} \text{ cm}^{-3}) \text{ esu}$  [ $\approx 3.4 \times 10^{-10} (N_3/10^{16} \text{ cm}^{-3}) \text{ SI}$ ], where the population  $N_3$  of state 3 changes between  $\sim (2-5) \times 10^{16} \text{ cm}^{-3}$  as the current increases.

Deep etched ridge waveguide lasers were processed in conventional fashion [6] with ridge widths ranging from

10 to 20  $\mu\text{m}$  and cleaved cavity lengths from  $\sim 1$  to 3 mm. The lasers were operated in pulsed mode with pulse widths ranging from 50 to 600 ns and at 1.8 to 85 kHz repetition rate. The laser output power was measured using a calibrated, room temperature HgCdTe photovoltaic detector. The laser spectra were measured using the rapid-scan mode of a Nicolet 860 Fourier transform infrared spectrometer (FTIR) and a liquid nitrogen (LN2) cooled HgCdTe photocurrent detector. The short wavelength radiation was measured using a calibrated, LN2 cooled InSb photovoltaic detector fitted with a sapphire flat to suppress the long wavelength radiation. The short wavelength spectra were obtained with the same detector and using the FTIR in step scan mode. We furthermore used a set of optical filters in the 4–6  $\mu\text{m}$  wavelength range to discriminate between the various components of the emitted radiation.

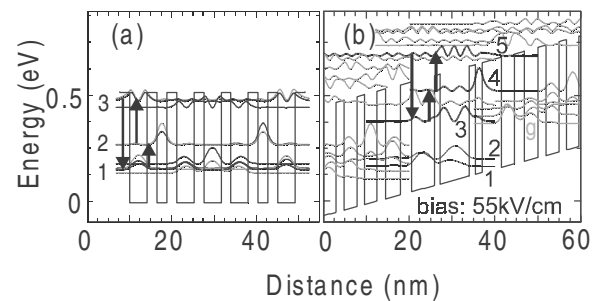


FIG. 1. (a), (b) Schematics of a portion of the conduction band diagram of the mixing SL and QC laser incorporating the optical nonlinearity, respectively. Shown also are the moduli squared of the relevant wave functions. In (a), the resonant nonlinearities result from transitions  $1 \rightarrow 2 \rightarrow 3$ . In (b), the QC-laser process is supported by levels 3, 2, and 1; the optical nonlinearities stem from resonant transitions  $3 \rightarrow 4 \rightarrow 5$ ; level g is the ground state of the injector region. Dotted lines in (b) indicate wave functions not directly involved in the laser or nonlinear processes. The solid arrows designate the nonlinear mixing process.

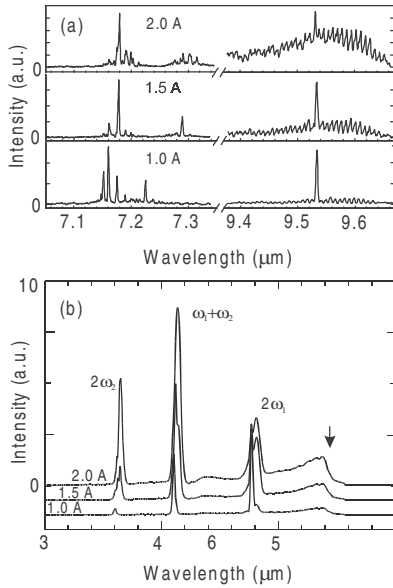


FIG. 2. (a) High resolution spectra measured of a  $10 \mu\text{m}$  wide and  $1.6 \text{ mm}$  long laser under pulsed operation at various levels of peak current as indicated. Individual longitudinal modes are broadened by thermal chirping, in particular, at high pulsed peak current levels. (b) Low resolution ( $1 \text{ meV}$ ) step-scan spectra of the same device measured under the same operating conditions in the short wavelength region. The spectra are offset with respect to each other, and the peaks are labeled in accordance with the main text. The small arrow indicates the spectral cutoff of one filter used in the experiment.

Figure 2(a) shows high-resolution spectra of a laser obtained at various levels of pumping current and at  $10 \text{ K}$  heat sink temperature. Figure 2(b) shows the corresponding short wavelength spectra. We observe sum and second-harmonic generation at  $4.1 (\omega_1 + \omega_2)$  and  $3.6$

( $2\omega_2$ ) and  $4.75 \mu\text{m} (2\omega_1)$ , respectively, at all pumping levels. We furthermore note a broad, slowly rising background, which we interpret as spontaneous emission from electrons excited into high lying energy levels and the continuum above the barriers.

In Fig. 3, the light output power and voltage versus current ( $L$ - $I$ - $V$ ) characteristics of the laser of Fig. 2 are shown, as well as the power of the nonlinearly generated radiation. The measurements have been taken at  $10 \text{ K}$  heat sink temperature. Laser threshold is reached at  $550 \text{ mA}$  approximately simultaneously for both wavelengths, and peak power is reached at  $2.6 \text{ A}$  with  $90$  and  $60 \text{ mW}$  for  $9.5$  and  $7.1 \mu\text{m}$  wavelength, respectively. Slightly beyond peak power, a sudden, strong increase in operating voltage occurs, indicative of a negative differential resistance region. We interpret this behavior as domain formation in the SL [16]. Such occurrence can be mitigated by higher doping or a modified design of the SL. Nevertheless, as can be seen in Fig. 3(d), the combined short wavelength emission reaches a power level of  $180 \text{ nW}$ . Figures 3(a)–3(c) show a detailed measurement of the optical power in each mixing component versus the power product of its generating laser sources. These data have been deduced from step scan spectra and the laser data of Fig. 3(d). The nonresonant background has been subtracted.

The results of our theoretical calculations are also shown in Figs. 3(a)–3(c). The power of each mixing signal has been obtained from solving the wave equation with the nonlinear polarization as a source, taking into account the phase mismatch of the waveguide modes and their losses due to diffraction and free-carrier absorption. The main contribution to the signal comes from the  $7.1 \mu\text{m}$  QC-laser region due to a much greater product of the three dipole moments. The resulting power in the  $\text{TM}_0$  mode of the sum-frequency signal at  $\lambda_3 = 4.1 \mu\text{m}$  can be estimated as

$$W_3 \sim \frac{128\pi^5 \Sigma^2 |\chi^{(2)}|^2 W_1 W_2 [1 + \exp(-2\alpha_3 L) - 2 \exp(-\alpha_3 L) \cos(\Delta k L)] (1 - R_3)}{\mu_1 \mu_2 \mu_3 c L_y \lambda_3^2 (\Delta k^2 + \alpha_3^2) (1 - R_1) (1 - R_2)}, \quad (2)$$

where  $\alpha_3$  stands for the total losses of cavity modes at  $\lambda_3 = 4.1 \mu\text{m}$ ,  $L$  for the cavity length, and  $R_{1,2,3}$  for the power reflection coefficients of the cavity at  $\lambda_{1,2,3}$ ;  $L_y = 10 \mu\text{m}$  is the lateral width of the waveguide,  $W_{1,2}$  is the power in the respective fundamental mode,

$$\Sigma = \frac{\mu_1 \mu_2}{\mu_3} \frac{\int \epsilon_3(x) \Phi_1 \Phi_2 \Phi_3 dx}{[\int \epsilon_1(x) \Phi_1^2 dx \int \epsilon_2(x) \Phi_2^2 dx \int \epsilon_3(x) \Phi_3^2 dx]^{1/2}}, \quad (3)$$

where  $\Phi_{1,2,3}(x)$  are the transverse distributions of the electric fields of modes participating in the nonlinear interaction,  $\epsilon_{1,2,3}(x)$  are the dielectric permittivities of a waveguide at wavelengths  $\lambda_{1,2,3}$ . The integral in the numerator of Eq. (3) is taken over the layers where  $\chi^{(2)}$  is different from zero, integrals in the denominator are from

$-\infty$  to  $+\infty$ , and we assume the fields to be homogeneous in the lateral  $y$  direction.

Waveguide losses of the nonlinear signal are mainly determined by near-resonant intersubband absorption and their value is below  $10 \text{ cm}^{-1}$  for electron densities below  $10^{17} \text{ cm}^{-3}$ . It is much smaller than the mismatch between the propagation constants of the three fields:  $\Delta k = k_3 - k_1 - k_2 \approx 600 \text{ cm}^{-1}$ ; i.e., the corresponding absorption length ( $0.1 \text{ cm}$ ) is much greater than the coherence length ( $\pi/\Delta k \sim 50 \mu\text{m}$ ). However, resonant losses may become an issue when we achieve phase-matched generation. In the present work, we did not do anything to improve the phase matching. However, due to a low dispersion of the waveguide in the midinfrared region, the values of effective refractive indices  $\mu_{1,2,3}$  are close to each other:  $\mu_1 = 3.259$ ,  $\mu_2 = 3.299$ ,  $\mu_3 = 3.354$ . This low dispersion is an

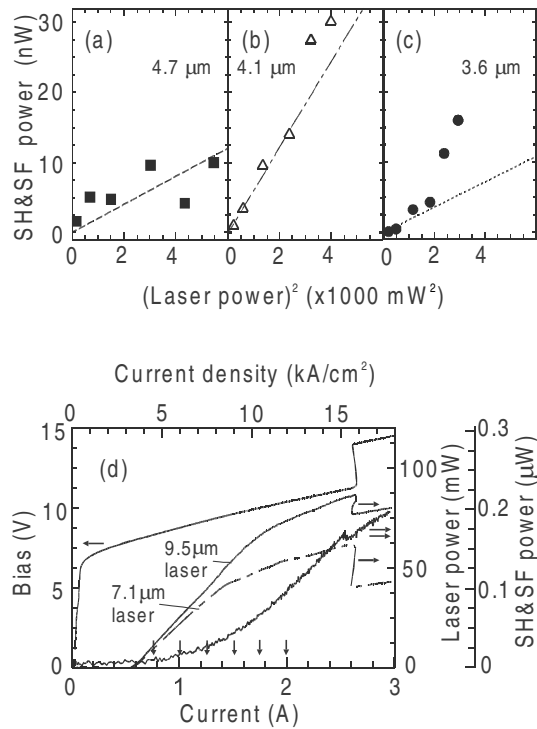


FIG. 3. (a)–(c) Optical power measured for sum-frequency (SF) [open triangles, (b)] and second-harmonic (SH) [filled circles and squares for 7.1 (c) and 9.5 μm (a), respectively] signals versus power squared of the respective fundamental pump light. The symbols represent data, the straight lines are our calculations. (d) Light-output and voltage versus current ( $L$ - $I$ - $V$ ) characteristic and combined short wavelength power of the laser of Fig. 2. The laser power has been split into its two wavelength components. The arrows pointing to the current axis indicate the positions where the spectra of Fig. 2 and the data points of (a)–(c) have been taken.

important advantage of QC lasers in intracavity wave mixing applications.

Similar formulas have been obtained for the second-harmonic signals. They are all shown in Figs. 3(a)–3(c) as theoretical curves, evaluated for  $N_3 = 4 \times 10^{16} \text{ cm}^{-3}$ , and are in good agreement with the data. The deviations at high pumping levels can be understood from several effects. First, as the current flow is increased through the structure, also the relative electron population of the upper laser level [“3” in Fig. 1(b)] increases; e.g., an increase of  $N_3$  to  $5 \times 10^{16} \text{ cm}^{-3}$  can already explain the deviation of the experimental curves [Figs. 3(b) and 3(c)] from straight lines at high powers. Another effect is the dependence of the dipole moments on the applied bias. This effect, especially important for dipole moment  $z_{54}$ , also leads to an excess of the mixing signal power as compared to the linear dependence. Finally, the frequencies of the IS transitions also depend on the applied bias. We calculate an increase of  $\omega_{43}$  with bias, while  $\omega_{54}$

decreases, both by a few meV over the range of applied electric fields deduced from the experiment (approximately 50–65 kV/cm). The susceptibility  $\chi^{(2)}$  at 3.6 μm is tuned to resonance with increasing  $\omega_{43}$ , while the one at 4.75 μm gets detuned from resonance. This can explain different behavior of the second-harmonic signals in Figs. 3(a) and 3(c).

We estimate that a waveguide design that incorporates considerations of phase matching, a larger electron population in the relevant energy levels, and improved optical dipole moments make an increase in the mixing signal power by 2–3 orders of magnitude feasible. Furthermore, the concepts discussed here for the generation of nonlinear light in QC lasers are general, and can in analogy be applied to a much wider range of QC-laser designs, including two-wavelength and multiwavelength QC lasers based on SL active regions [17]. Finally, the designs discussed here may also provide fundamentally new approaches to the realization of other coherent nonlinear optical sources.

The work performed at Bell Laboratories was partly supported by DARPA/US ARO under Contract No. DAAD19-00-C-0096. A. B. and V. K. acknowledge the support from Texas Advanced Research and Technology Program and the Office of Naval Research.

- [1] S. E. Harris and A. V. Sokolov, Phys. Rev. Lett. **81**, 2894 (1998).
- [2] Yu. Rostovtsev, O. Kocharovskaya, G. R. Welch, and M. O. Scully, Opt. Photonics News **13**, 44 (2002).
- [3] M. Saba *et al.*, Nature (London) **414**, 731 (2001).
- [4] N. Gisin, G. Ribordy, W. Tittel, and H. Zbinden, Rev. Mod. Phys. **74**, 145 (2002).
- [5] K. J. Resch, J. S. Lundeen, and A. M. Steinberg, Phys. Rev. Lett. **87**, 123603 (2001).
- [6] C. Gmachl, F. Capasso, D. L. Sivco, and A. Y. Cho, Rep. Prog. Phys. **64**, 1533 (2001).
- [7] M. K. Gurnick and T. A. DeTemple, IEEE J. Quantum Electron. **19**, 791 (1983).
- [8] M. M. Fejer, S. J. B. Yoo, R. L. Byer, A. Harwit, and J. S. Harris, Phys. Rev. Lett. **62**, 1041 (1989).
- [9] P. Boucaud *et al.*, Appl. Phys. Lett. **57**, 215 (1990).
- [10] F. Capasso, C. Sirtori, and A. Y. Cho, IEEE J. Quantum Electron. **30**, 1313 (1994).
- [11] M. J. Shaw *et al.*, Phys. Rev. B **50**, 18395 (1994).
- [12] H. C. Liu, E. Costard, E. Rosencher, and J. Nagle, IEEE J. Quantum Electron. **31**, 1659 (1995).
- [13] E. Rosencher *et al.*, Science **271**, 168 (1996).
- [14] A. A. Belyanin *et al.*, Phys. Rev. A **63**, 053803 (2001); **65**, 053824 (2002).
- [15] C. Gmachl *et al.*, Appl. Phys. Lett. **79**, 572 (2001).
- [16] H. T. Grahn, R. J. Haug, W. Müller, and K. Ploog, Phys. Rev. Lett. **67**, 1618 (1991).
- [17] A. Tredicucci *et al.*, Nature (London) **396**, 350 (1998).